Lateral spacing of adhesion peptides influences human mesenchymal stem cell behaviour

Jessica E. Frith[1], Richard J. Mills[1] and Justin J. Cooper-White[1,2,*]

[1]Tissue Engineering and Microfluidics Laboratory, Australian Institute for Bioengineering and Nanotechnology, University of Queensland, Queensland, 4072, Australia
[2]School of Chemical Engineering, University of Queensland, Queensland, 4072, Australia
*Author for correspondence (j.cooperwhite@uq.edu.au)

Accepted 27 August 2011
Journal of Cell Science 125, 317–327

doi: 10.1242/jcs.087916

Summary

Mesenchymal stem cells (MSCs) have attracted great interest in recent years for tissue engineering and regenerative medicine applications due to their ease of isolation and multipotent differentiation capacity. In the past, MSC research has focussed on the effects of soluble cues, such as growth factors and cytokines; however, there is now increasing interest in understanding how parameters such as substrate modulus, specific extracellular matrix (ECM) components and the ways in which these are presented to the cell can influence MSC properties. Here we use surfaces of self-assembled maleimide-functionalized polystyrene-block-poly(ethylene oxide) copolymers (PS-PEO-Ma) to investigate how the spatial arrangement of cell adhesion ligands affects MSC behaviour. By changing the ratio of PS-PEO-Ma in mixtures of block copolymer and polystyrene homopolymer, we can create surfaces with lateral spacing of the PEO-Ma domains ranging from 34 to 62 nm. Through subsequent binding of cysteine–GRGDS peptides to the maleimide-terminated end of the PEO chains in each of these domains, we are able to present tailored surfaces of controlled lateral spacing of RGD (arginine-glycine-aspartic acid) peptides to MSCs. We demonstrate that adhesion of MSCs to the RGD-functionalized block-copolymer surfaces is through specific attachment to the presented RGD motif and that this is mediated by α5, αV, β1 and β3 integrins. We show that as the lateral spacing of the peptides is increased, the ability of the MSCs to spread is diminished and that the morphology changes from well-spread cells with normal fibroblastic morphology and defined stress-fibres, to less-spread cells with numerous cell protrusions and few stress fibres. In addition, the ability of MSCs to form mature focal adhesions is reduced on substrates with increased lateral spacing. Finally, we investigate differentiation and use qRT-PCR determination of gene expression levels and a quantitative alkaline phosphatase assay to show that MSC osteogenesis is reduced on surfaces with increased lateral spacing while adipogenic differentiation is increased. We show here, for the first time, that the lateral spacing of adhesion peptides affects human MSC (hMSC) properties and might therefore be a useful parameter with which to modify hMSC behaviour in future tissue engineering strategies.

Key words: Mesenchymal stem cell, RGD peptide, Cell morphology, Differentiation, Nanopatterning

Introduction

Adherent cells respond to a large number of cues provided by the physical extracellular environment. The principal link between the cell and the extracellular environment is provided by membrane-spanning integrins, which bind both to specific motifs in the surrounding extracellular matrix (ECM) and to a number of proteins within the cell. Upon binding, integrins cluster and proteins including talin, paxillin and vinculin are recruited to form focal adhesions (FAs) (Critchley, 2000). These dynamic and complex assemblies fulfil a mechanical role as they connect to the actin cytoskeleton, providing an anchor point from which the cytoskeleton can generate cellular tension (Balaban et al., 2001). However, because FAs contain proteins that interact with chemical signalling pathways, such as Rac, RhoA and Cdc42 (Ren et al., 1999; Geiger and Bershadsky, 2001; Riveline et al., 2001), they also serve as signalling centres linking mechanical signals to soluble intracellular signalling cascades. It is through these mechanisms that cells interpret the environment around them and respond via changes in cell spreading, morphology and migration.

These principles also apply to mesenchymal stem cells (MSCs), which are multipotent progenitor cells that have attracted great interest for tissue engineering and regenerative medicine applications. Previous studies have determined that cues from the physical environment can influence MSCs, affecting both their growth and ability to differentiate along different lineages. For example, MSC behaviour has been shown to be influenced by substrate elasticity (Engler et al., 2006; Rowlands et al., 2008; Winer et al., 2009; Cameron et al., 2011), geometry (Cukierman et al., 2001), extracellular matrix (ECM) composition (Kundu and Putnam, 2006; Rowlands et al., 2008) and topography (Kantawong et al., 2009; Yim et al., 2010). This fits well with the concept of the stem cell niche in which factors from the local environment including soluble signals, cell–cell contacts and physical cues all interact to regulate stem cell fate. It is thus imperative that we gain a greater understanding of the different facets of the cellular microenvironment and the way that they influence MSCs if we are to develop optimal strategies for MSC expansion and tissue engineering applications.

Journal of Cell Science

Although great advances have been made in understanding how various parameters of the extracellular environment affect MSC properties, these have only progressed as fast as our ability to modulate and specifically control different aspects of the external environment. In line with advances in biomaterials and surface engineering, studies have moved from investigations into how different ECM molecules affect MSCs, (Salasznyk et al., 2004; Klees et al., 2005; Kundu and Putnam, 2006) to those that have allowed us to probe the influence of individual ECM domains or peptide motifs (Martino et al., 2009), substrate modulus (Engler et al., 2006; Winer et al., 2009), substrate creep (Cameron et al., 2011), cell shape and spread (McBeath et al., 2004) and position within a multicellular aggregate (Nelson et al., 2005; Ruiz and Chen, 2008) or combinations of these factors (Rowlands et al., 2008; Kilian et al., 2010).

The most recent breakthrough has been the development of substrates that enable ligands to be presented to cells with control of spatial organization at the nanometre level (Arnold et al., 2004; George et al., 2009b). This level of organization is thought to be important because ECM molecules are multifaceted, containing multiple domains with repeated motifs whose presentation to the cell is both complex and can be changed by protein folding and unfolding (Poole et al., 2005; Martino et al., 2009). We also know that the ability of integrins to cluster, a necessary prerequisite for recruitment of proteins to the FA complex, is affected by spacing of the presented ligand and has downstream consequence for integrin-linked signalling cascades (Irvine et al., 2002; Selhuber-Unkel et al., 2008). Work by the Spatz group has demonstrated that cells do sense and respond to changes in lateral spacing of ligands on the nanoscale, with changes observed in cellular adhesion, spreading and morphology (Arnold et al., 2004; Cavalcanti-Adam et al., 2006; Cavalcanti-Adam et al., 2007; Arnold et al., 2008; George et al., 2009b). This work has so far been limited to committed cell types. However, due to the fact that MSC properties are so sensitive to other features of the physical environment, we hypothesized that they would also be affected by the lateral spacing of presented ECM signals.

Previous work in our group has shown that through the self-assembly of poly(styrene-block-ethylene oxide) (PS-PEO) block copolymers, it is possible to produce micro-phase separated surfaces consisting of separated, vertically oriented cylinders constituted of a defined number of PEO chains (or tethers) in a matrix of PS. Furthermore, the lateral spacing of these clustered PEO chains (PEO domains) can be controlled via the use of different blends of PS-PEO and polystyrene (PS) homopolymer (George and Cooper-White, 2009; George et al., 2009a). Through modification of the terminal alcohol of the PEO block it is then possible to functionalize the PEO tethers within these separated domains with cell adhesion motifs, thus providing a platform with which to present domains or clusters of adhesion peptides with different lateral spacings (George et al., 2009b). Importantly, the length scales of these domains are such that only one integrin can ligate with a cell adhesion motif presented within each domain. Here we use this simple, but highly reproducible technique to present a substrate with defined spacing of RGD (arginine-glycine-aspartic acid) peptides to human MSCs (hMSCs). We investigate how this influences MSC behaviour, showing for the first time that changes in the lateral spacing of cell adhesion motifs affects hMSC morphology, migration and differentiation characteristics.

Results

MSCs adhere specifically to peptides presented on PEO nanodomains via α5, αV, β1, β3 and β5 integrins

Adhesion assays were performed to quantify hMSC attachment to RGD-functionalized PS-PEO-maleimide (PS-PEO-Ma) surfaces and probe the specificity of such interactions (Fig. 1A). hMSC adhesion to RGD peptides presented on the PS-PEO-Ma surface was at a level similar to that on tissue culture plastic (TCP). However, there was no adhesion either to PS-PEO-Ma alone or when functionalized with a cryptic RGE peptide. Furthermore, no adhesion was evident on PS alone or on PS surfaces that had been incubated with RGD peptide, indicating that hMSC adhesion was not mediated by physisorption of RGD to the PS surface and that adhesion was mediated specifically by interactions with RGD peptides presented on the PEO domain of the PS-PEO-Ma.

Integrin expression profiling of the hMSCs used in this study showed that a high proportion of the hMSC population expressed integrins α1–α5 and αV as well as β1 integrin and a smaller percentage expressed integrins α6 and β3–β5, with high levels of integrins α3, α5, αV and β1 (supplementary material Fig. S1). To determine the primary interactions between the hMSCs and the presented RGD peptides, integrin blocking experiments were performed. Due to the expression levels observed in the hMSC population and the integrin subunits known to interact with RGD (Ruoslahti, 1996), antibodies specific to integrins α5, αV, β1, β3 and β5 were used. These experiments confirmed that integrins α5, αV, β1, β3 and β5, or combinations of these integrins, significantly reduced the adhesion of hMSCs, with the greatest reduction in attachment seen when blocking all of these integrins together (Fig. 1B).

Lateral spacing of adhesion peptides affects hMSC morphology, FA formation and cytoskeletal organization

Surfaces were prepared using blends of PS-PEO-Ma with PS to present RGD domains having an average lateral spacing of 34, 44, 50 or 62 nm (supplementary material Fig. S2). hMSCs were seeded onto these substrates and after 4 hours had attached and spread. Measurements of projected cell area showed that hMSCs cultured on RGD domains spaced at 50 and 62 nm had significantly smaller spread areas than those on either 34-nm- or 44-nm-spaced RGD domains (Fig. 2A). The hMSCs also showed different morphologies depending upon the spacing of the RGD domains, with a progression from well-spread cells on 34-nm-spaced RGD domains, to cells extending multiple filopodia on the 62-nm-spaced RGD domains (Fig. 2B). There were also differences in the organization of the actin cytoskeleton, with hMSCs on the 34-nm- and 44-nm-spaced peptide domains possessing large, well-defined stress fibres whereas cells on the 50-nm-spaced and particularly the 62-nm-spaced peptide domains had a more disorganized actin cytoskeleton consisting of a widely branched network of thin fibres and numerous individual filaments extending from the main body of the cell (Fig. 2B). Immunostaining for focal adhesion kinase (FAK) also showed decreased expression in hMSCs with lateral RGD domain spacing of 50 nm and above (Fig. 2B).

In order to confirm that the observed differences were due to the lateral spacing of the presented RGD peptide domains and not simply a result of changes in the absolute surface density of RGD, we next prepared PS-PEO-Ma substrates with an average PEO domain spacing of 34 nm that were subsequently

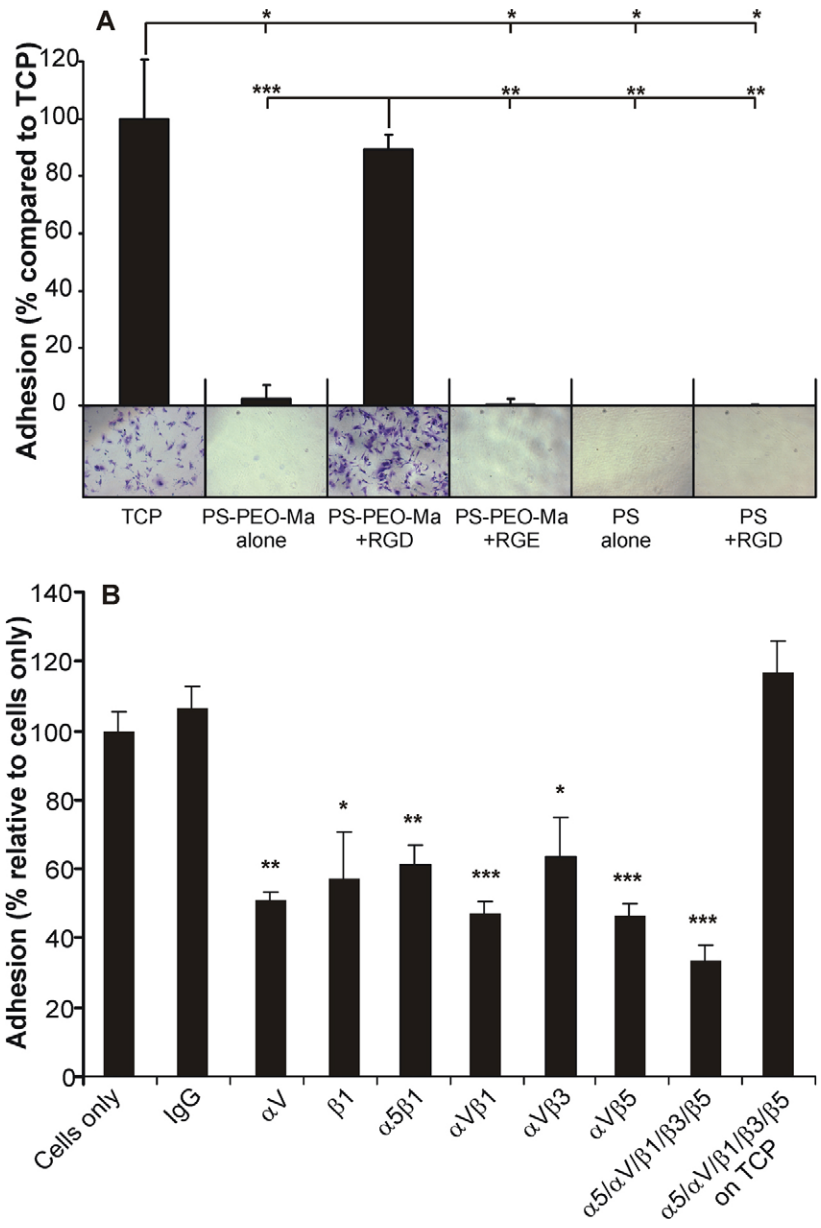

Fig. 1. Adhesion of hMSCs to peptides presented on PS-PEO-Ma surfaces. (**A**) Adhesion assay showing hMSC attachment to PS-PEO-Ma or PS surfaces, alone or functionalized with RGD and RGE peptides. (**B**) Integrin blocking of hMSCs on PS-PEO-Ma–RGD. Data is presented as mean percentage + s.e.m.; $n=3$, $^{*}P<0.05$, $^{**}P<0.01$, $^{***}P<0.001$.

functionalized with differing ratios of RGD to RGE peptide. Calculation of the radius of gyration of the PEO block showed that an average of six PEO tethers are clustered together in each of the PEO cylinders (domains) presented in the PS background. Assuming that the attachment of either RGD or RGE to each PEO tether is random, it is therefore only between RGD dilutions of 1:8 and 1:16 (where the average number of adhesive RGD peptides per PEO domain is less than one) that the distance between effective adhesive sites is changed (supplementary material Fig. S3). Until this point, integrins can cluster over similar length scales (even though the absolute surface concentration of RGD is reduced) due to the fact that only one integrin can bind to any adhesive peptide presented on each PEO domain.

After 4 hours of culture on surfaces functionalized with dilutions of up to 1:16 RGD in RGE (Fig. 3A), there were no significant differences in cell spread area between hMSCs, whereas changes in the lateral spacing of the RGD (only) functionalized PEO domains from 34 to 62 nm, which resulted in the global RGD density decreasing by a factor of less than four (from ~4500 to 1560 peptides/μm^2), produced substantial reductions in the spread area of hMSCs that were significantly different ($P<0.001$). Furthermore, although there was some evidence of a decrease in the number of stress fibres in hMSCs cultured on surfaces functionalized with 1:8 and 1:16 RGD, these changes were much less prominent than those observed with increased lateral spacing of RGD domains (Fig. 3B). This is due to the fact that some of the domains presenting RGD will still be spaced at 34 nm apart in groupings that allow integrin clustering even at these dilution levels (supplementary material Fig. S3). Overall, the cellular changes seen across this dilution series were certainly not as substantial as those seen through systematic changes in the lateral spacing of adhesive PEO domains presenting only RGD peptides. This confirmed that the

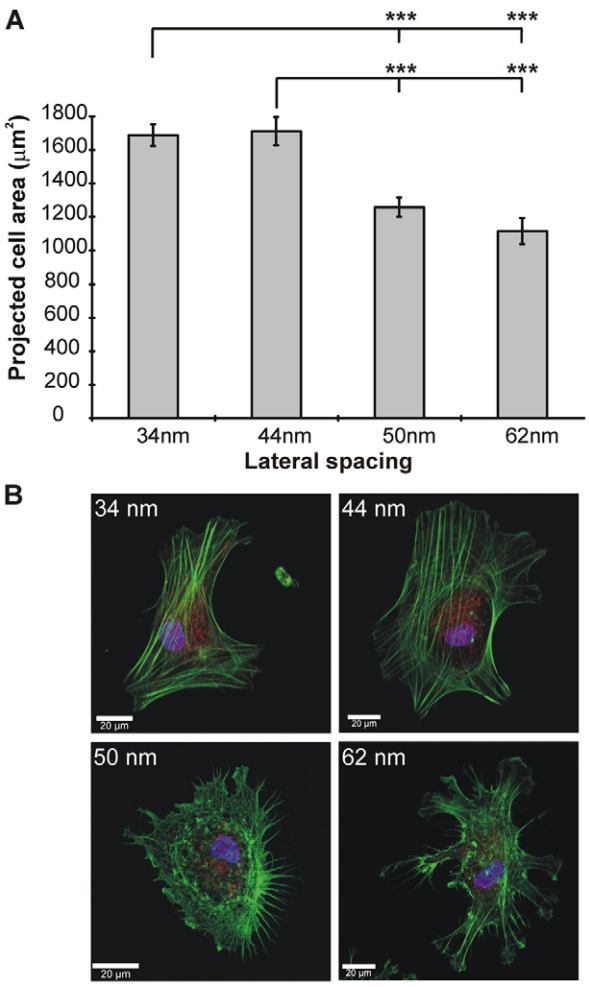

Fig. 2. Lateral spacing of RGD peptides affects hMSC spread area, morphology and cytoskeleton organization. (**A**) Projected cell area of hMSCs on peptides of different spacing. Data is presented as mean ± s.e.m. $n>100$. Statistical significance was determined by Mann-Whitney *U*-test using the Bonferroni constant to adjust for multiple comparisons; ***$P<0.001$. (**B**) hMSCs stained for actin (green), Hoechst 33342 (blue) and FAK (red) after 4 hours culture of PS-PEO surfaces. Scale bars: 20 μm.

observed effects were primarily the result of the differences in lateral spacing of the adhesive peptide and not the differences in adhesive peptide surface density.

Due to the substantial changes we observed in the organization of actin cytoskeleton as the lateral spacing of RGD peptide increased, we next examined whether there were further changes to the cytoskeletal architecture, in particular to FA formation. Vinculin immunolocalization was used to detect matrix adhesions and, after 24 hours of culture, hMSCs on the 34-nm- and 44-nm-spaced peptide had large, discrete vinculin-positive complexes. However, in hMSCs on the 50-nm- and 62-nm-spaced peptide these complexes were much smaller and, in contrast to those on the more closely spaced peptide, were not localized to the ends of actin filaments (Fig. 4A,B). Measurements of vinculin complex length determined that hMSCs on 34-nm-spaced peptides had a significantly higher proportion of vinculin complexes with a length of 10 μm or longer, indicative of fully mature FAs (Riveline et al., 2001), than hMSCs on 62-nm-spaced peptides. The inverse was true for nascent focal complexes of less than 5 μm in length, which were significantly more prevalent in hMSCs on 62-nm- than 34-nm-spaced RGD (Fig. 4C).

hMSC migration is influenced by lateral spacing of RGD peptide

Given the changes to cytoskeletal morphology and FA formation, we hypothesised that hMSC migration might be influenced by RGD spacing. To establish whether this was true, we used a microchannel migration device (Doran et al., 2009) to determine the migration rate of hMSCs on surfaces with different RGD spacings. The migration rate of the hMSCs was seen to increase as the spacing of the RGD increased from 34 to 50 nm, leading to a significantly higher migration speed on 50-nm-spaced peptides than on 34-nm-spaced peptides. For example, the rate for hMSCs from one donor increased from an average migration rate of 7.7 μm/hour to 12.3 μm/hour. This migration rate then decreased on surfaces with 62-nm-spaced RGD to a rate of 10.9 μm/hour, leading to a parabolic trend in migration rate over the four differential peptide spacings (Fig. 5).

Osteogenic and adipogenic differentiation are influenced by lateral spacing of RGD peptide

We next wanted to determine whether changes in the lateral spacing of RGD would influence hMSC differentiation. hMSCs were allowed to attach to the different substrates for 4 hours in the absence of serum before the media was replaced with either osteogenic or adipogenic (serum-containing) media. After 7 days of osteogenic differentiation, there were no significant differences in the expression level of Runx2 (Fig. 6A); however, alkaline phosphatase activity was significantly reduced (by 30%) in MSCs on the 62-nm- as compared with those on 34-nm-spaced RGD (Fig. 6B). Alizarin Red staining after 10 days of differentiation showed greater mineral deposition in hMSCs on 34-nm- than on 62-nm-spaced RGD (Fig. 6C). Conversely, in adipogenic cultures, the relative expression levels of the adipogenic markers PPARγ and LPL were significantly upregulated (by 48% and 288%, respectively) in hMSCs on 62-nm-spaced RGD after 7 days of differentiation, as compared with 34-nm-spaced RGD (Fig. 6D,E). In addition, Oil Red O staining showed increased amounts of lipid droplet accumulation on 62-nm-spaced RGD after 10 days of differentiation (Fig. 6F).

To determine whether the lateral spacing of RGD would affect the lineage specification of hMSCs when provided with signals sufficient to induce both osteo- and adipogenic differentiation, hMSCs seeded onto either 34-nm- or 62-nm-spaced peptides were cultured in a mixed media containing equal amounts of both osteo- and adipogenic media. After 10 days, a significantly increased proportion of hMSCs on the 34-nm-spaced RGD showed alkaline phosphatase expression as compared with those on the 62-nm-spaced RGD. Conversely, there was a significantly greater number of Oil Red O-positive hMSCs on the 62-nm-, as compared with the 34-nm-spaced RGD (Fig. 7A,B).

Discussion

We have used self-assembled PS-PEO-Ma surfaces, functionalized with RGD peptide, to determine the effect of lateral spacing of cell adhesion ligand on hMSC behaviour and showed that changing the lateral spacing affected

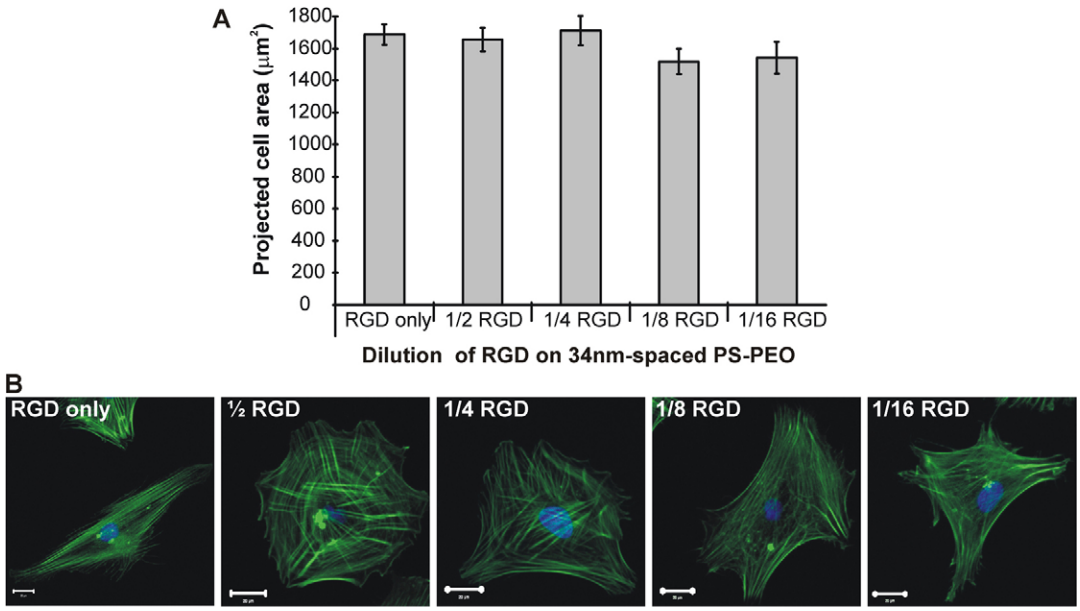

Fig. 3. Projected cell area and morphology of hMSCs on PS-PEO surfaces functionalized with increasing dilutions of RGD in RGE. (**A**) Projected cell hMSCs on PS-PEO surfaces functionalized with different dilutions of RGD peptide. These ranged from surfaces functionalized with RGD only to those functionalized with a 1:16 dilution of RGD in RGE. Statistical significance was determined by Mann-Whitney *U*-test using the Bonferroni constant to adjust for multiple comparisons; $*P<0.05$. (**B**) hMSCs stained for actin (green) and Hoechst 33342 (blue) after 4 hours culture on PS-PEO surfaces. Scale bars: 20 μm.

hMSC morphology, cytoskeletal organization, migration and differentiation.

We first confirmed that hMSC adhesion to the PS-PEO surfaces was mediated via interactions with the presented RGD and that the RGD was presented specifically on the PEO nanodomains. hMSCs adhered to RGD-functionalized PS-PEO-Ma surfaces with a similar efficiency as to TCP. However, the lack of attachment to either non-functionalized or RGE-functionalized PS-PEO-Ma confirmed that cell adhesion was specifically mediated via the RGD peptide and that hMSCs could not attach to the PS-PEO-Ma alone. PS alone, even when incubated with RGD peptide, would not facilitate cell attachment showing that simple physisorption of peptide to the PS background was not responsible for hMSC adhesion. The specificity of the interaction with the RGD peptide was also confirmed, with integrin-blocking experiments showing that adhesion was facilitated by the common RGD-binding integrins α5, αV, β1, β3 and β5 (Ruoslahti, 1996).

Having confirmed the specificity of interactions between hMSCs and RGD peptides presented on the PEO domains, we then used surfaces prepared using different blends of PS-PEO-MA and PS to investigate the effect of RGD spacing on hMSC properties. Previous work from our group has shown that the lateral spacing of PEO domains in a surface can be altered by blending PS-PEO-Ma with PS monomer (George et al., 2009b) and that the average spacing of the PEO nanodomains can be increased from 34 to 62 nm by reducing the proportion of PS-PEO-Ma in the blend down to 25%. Importantly, because the size of these PEO nanodomains is limited to 14 nm (George and Cooper-White, 2009), which is approximately the size of an individual integrin (Hynes, 1992), this means that only one integrin in the cell membrane can interact with the peptide presented on any one nano-island. This therefore provided us with the ideal platform with which to investigate the effects of adhesion peptide spacing on hMSC properties. It should be noted, however, that the force of the cell binding to presented peptides can result in extension of PEO tethers (Kuhlman et al., 2007). This could mean that the distance between adjacent RGD peptides in our system did not remain constant (at 34 or 62 nm for example) after the binding of integrins to the presented peptides, as a result of cytoskeletal reorganization within the cell. It seems unlikely, however, that a large degree of PEO extension occurred in our experiments because a comparison with work using rat embryonic fibroblasts by the Spatz group (Cavalcanti-Adam et al., 2006; Cavalcanti-Adam et al., 2007) (which did not use PEO tethers as a base for peptide presentation) showed similar morphological and FA changes over similar lateral length scales of peptide presentation. The lateral spacings presented here in this work (whether changed by PEO tether extension or not) are clearly sufficient to reveal differences in hMSC behaviour.

Analyses of hMSC morphology showed that cell spread area decreased when the lateral spacing of the RGD reached 50 nm or more. In addition, there were cytoskeletal changes associated with increased lateral spacing, resulting in hMSC on the 62-nm-spaced RGD having a highly disorganized actin cytoskeleton. The 34-nm-spaced surfaces functionalized with different ratios of RGD and RGE were used to confirm that these changes in cell behaviour were not due to changes in RGD density alone but a result of differences in lateral spacing of RGD peptide domains.

Although ligand density can affect cellular properties (Massia and Hubbell, 1991; Chollet et al., 2009), this conclusion is also supported by other work in which the relationship between global ligand density and ligand presentation has been studied. An elegant study by Maheshwari and co-workers (Maheshwari et al., 2000) used star polymers to present either single RGD peptides or clusters of five and nine peptides at different lateral spacings. Although differences were observed as the average ligand density changed, they showed that much larger spacing of the clusters

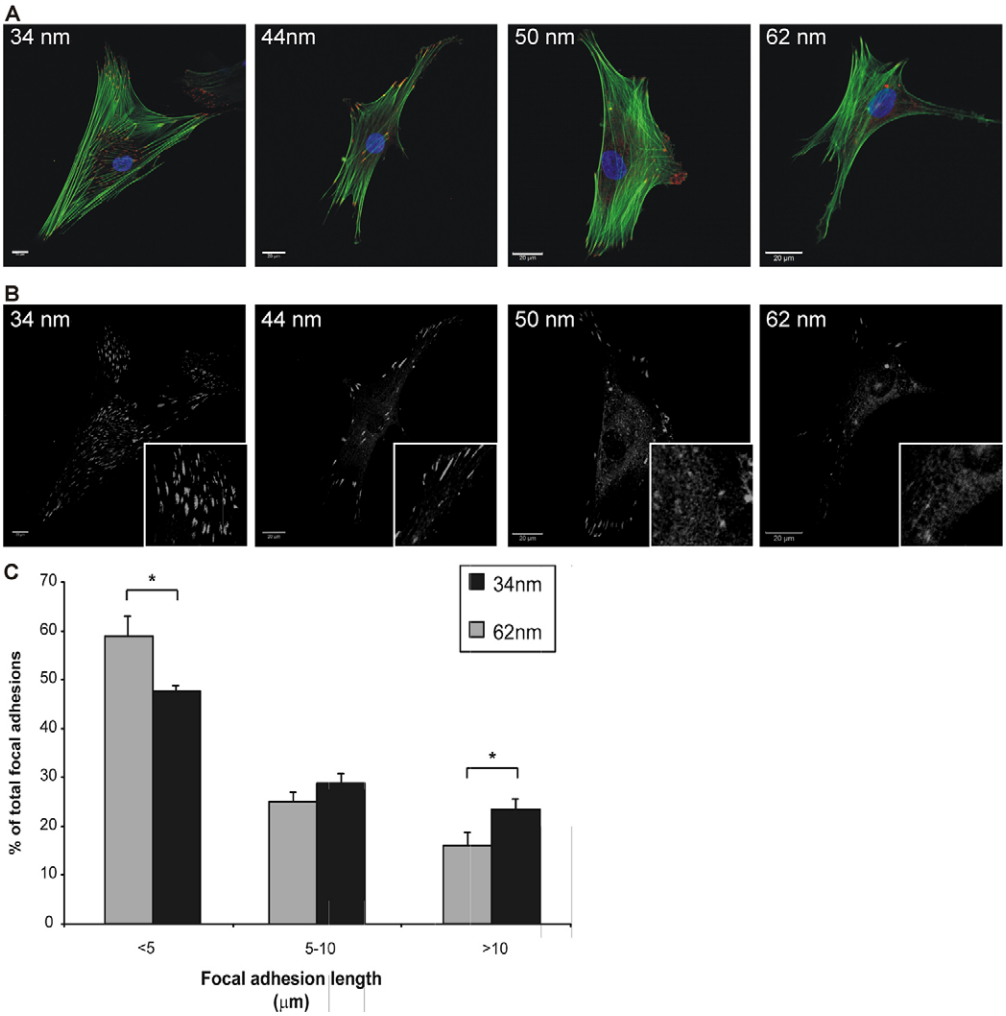

Fig. 4. Lateral spacing of RGD peptides affects FA formation. (**A**) hMSCs stained for actin (green), Hoechst 33342 (blue) and Vinculin (red) after 4 hours culture on PS-PEO-Ma–RGD surfaces. (**B**) Black and white images show vinculin staining alone for the same cell with enlarged images (inset). Scale bars: 20 μm. (**C**) Measurements of FA length. Data is presented as mean percentage of total FAs in each size range + s.e.m. for hMSCs from three independent donors; $n>3000$, $*P<0.05$.

could be tolerated (without inducing any change to the cells) when the number of ligands in the cluster was increased and that differences in the clustering of the ligands produced differences in cell morphology and migration even when the global ligand density remained unchanged. Micro- and nanopatterned surfaces have also been used to alter local ligand density without affecting global ligand density, confirming that local ligand density (and therefore ligand spacing) is important (Arnold et al., 2004; Arnold et al., 2009). Indeed, if the density of these ligands is compared with densities in the current study, global ligand densities of just 90 RGD peptides/μm^2 (which is much below our lowest density of 260 peptide domains/μm^2, each domain being constituted of about six peptides) were shown not to interfere with cell spreading when the local spacing was kept below 58 nm (Arnold et al., 2004).

In addition to the change in cell spread area and actin organization, hMSCs cultured on 62-nm-spaced RGD also had a reduced proportion of large, mature FAs and an increased number of nascent focal complexes as compared with those on 32-nm-spaced RGD. Together, these morphological changes are consistent with studies using fibroblasts or other committed cell types in which the length scale at which cells could no longer adhere, spread and form an organized cytoskeleton with stable, mature FAs was determined to be over 73 nm (Arnold et al., 2004; Cavalcanti-Adam et al., 2006; Cavalcanti-Adam et al., 2007; Huang et al., 2009). Binding of integrins to ligands induces a conformational change in the structure of the cytoplasmic tail of the integrin, which initiates integrin clustering (Humphries et al., 2003) and provides a core from which α-actinin, talin and vinculin bind and focal complexes then build. A critical number of integrins are required to cluster before this can happen, with different studies proposing a grouping of either five (Maheshwari et al., 2000) or six integrins (Arnold et al., 2009) as the necessary threshold. It is hypothesized that substrates with peptide presented with lateral spacing greater than ~70 nm do not allow the necessary number of integrins to cluster and initiate this process. This might also explain why cellular responses to a change in the overall ligand concentration can differ depending on whether the peptides are presented randomly or as clusters (Maheshwari et al., 2000). Interestingly, although our data support these hypotheses, we observed a reduction in mature FA formation with a lateral spacing of 62 nm, which is smaller than that previously reported. This value lies between spacings used in other studies and so might represent a distance closer to the actual threshold at which integrin clustering cannot occur, at least for hMSCs. However, at this distance we observed a reduction on the proportion of mature FAs and not a complete abolition of FA formation. Huang and co-workers (Huang et al., 2009)

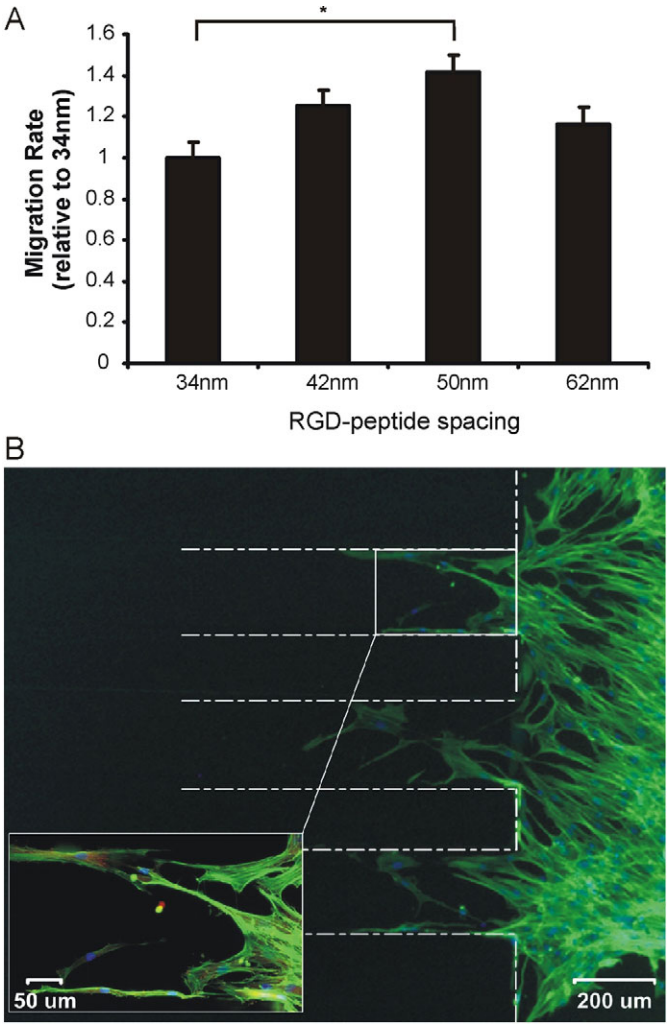

Fig. 5. hMSC migration rate on substrates with different lateral spacing of RGD peptide. (**A**) Migration rates of hMSCs on substrates with different lateral spacing of peptides. Data is presented as mean + s.e.m. relative to hMSCs on 34-nm-spaced surfaces for hMSCs from three independent donors; *$P<0.05$. (**B**) Example of hMSC migration on 42-nm-spaced RGD. hMSCs are stained for actin (green), Hoechst 33342 (blue) and vinculin (red).

demonstrated different thresholds for FA formation when ligands were presented in ordered or disordered patterns, suggesting that by chance some areas on disordered patterns allow the clustering of enough integrins for FA formation even when the average spacing was above 70 nm. Our substrates more closely match this disordered substrate, having a distribution of interdomain spacings (supplementary material Fig. S2C), and so the fact that some mature FAs were observed on 62-nm-spaced RGD is probably due to local variations in the ligand density. The application of force is also required for FA maturation (Balaban et al., 2001; von Wichert et al., 2003) and so there is a requirement for a strong attachment to the underlying substrate to allow mechanically stable adhesions to form. The strength of cell attachment has been shown to change with differences in ligand spacing (Selhuber-Unkel et al., 2010), and so it might be that, in a manner similar to cells cultured on very soft (elastic) substrates, the strength of the connection to the substrate is not sufficient on substrates with increased lateral spacing of ligand to support the required levels of force for focal complex maturation.

FAs are key centres for anchorage and organization of the actin cytoskeleton and so the observed changes to cytoskeletal organization are likely to be associated with the altered proportions of immature focal complexes and mature FAs. There are two mechanisms through which this could influence cytoskeletal assembly. Firstly, the lack of stress fibres in hMSCs on 62-nm-spaced RGD might be a consequence of the adhesions being too weak to support the force applied by stress fibres, although changes in actomyosin contractility also feed back into regulation of FA maturation (Choi et al., 2008) and so, in turn, have an effect on FA formation. Secondly, cytoskeletal formation is also governed by the specific composition of the FA. In addition to proteins playing a role as adaptor or scaffolding units, many components have enzymatic activity whose signalling regulates actomyosin assembly. In particular, RhoA, which is known to promote both FA maturation and stress fibre formation, is regulated by the activity of GTPase activating proteins (GAPs) and guanine nucleotide exchange factors (GEFs), which are both recruited to and regulated by components of the adhesion complex (Schober et al., 2007). Due to the decreased FA and stress fibre formation in hMSCs on the 62-nm-spaced RGD, it is likely that reduced RhoA activity, as a result of altered focal complex composition, leads to changes in cytoskeletal organization (Ridley and Hall, 1992). In support of this hypothesis, differences in FA composition have been documented as lateral spacing of adhesion peptide was increased in other cell types (Cavalcanti-Adam et al., 2007).

We hypothesized that the morphological changes (cell spreading, cytoskeletal architecture and FA formation) induced by differences in ligand spacing would also affect cellular functions such as migration and differentiation. Cell migration speed over a substrate is known to be dictated through short-term cell–substrate adhesiveness. Palecek and co-workers demonstrated that ligand concentration, integrin expression and their binding affinity control the cell attachment force to the substrate, which in turn determines the migration speed (Palecek et al., 1997). Therefore, high cell–substratum adhesiveness hinders cell migration by obstructing release of adhesions, whereas low cell–substratum adhesiveness leads to unstable lamellipodal extensions. Maximum cell migration therefore occurs at intermediate adhesion strengths. Given that intermolecular spacing of adhesion receptors governs cell adhesion strength (Selhuber-Unkel et al., 2010), and with the changes we observed in FA formation on the different substrates, we hypothesized that migration rates would differ due to differing adhesion strengths on the different RGD spacings. Our data showed an increase in migration rate with spacings between 34 and 50 nm, with a subsequent decrease on 62-nm-spaced RGD. We propose that migration rate increases with spacings between 34 and 50 nm as adhesion strengths move closer to the optimum, incorporating sufficient strength to support the cell but also with efficient turnover. The adhesion strength of the immature adhesions on 62-nm-spaced RGD is likely to lead to less stable protrusions and therefore to slower migration. This is supported by previous work in which REF52 cells showed erratic movements on surfaces with large lateral spacing of peptides (Cavalcanti-Adam et al., 2007), a factor we have also observed in time-lapse movies of hMSCs in this study (data not shown). The observed differences in hMSC migration

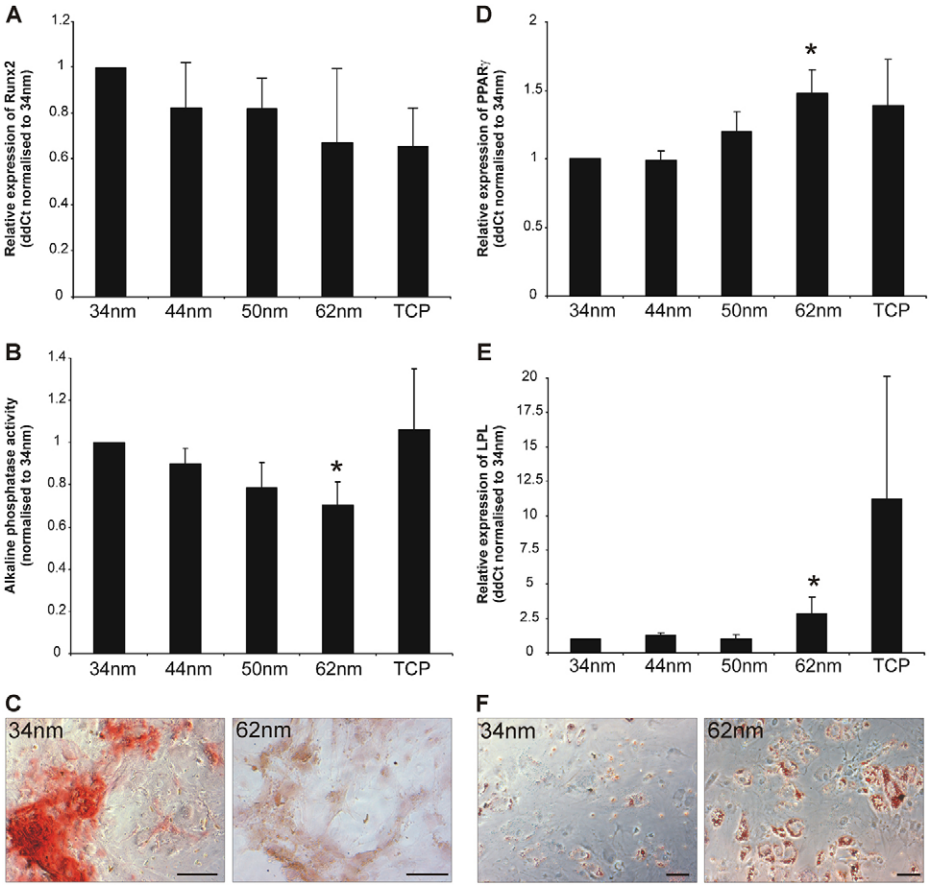

Fig. 6. Differentiation of hMSCs on different RGD peptide spacings. (**A**) qPCR determination of Runx2 expression and (**B**) alkaline phosphatase activity in hMSCs after 7 days of osteogenic induction. (**D**) qPCR determination of PPARγ and (**E**) LPL expression after 7 days of adipogenic induction. Data is presented relative to levels in hMSCs cultured on 34-nm-spaced surfaces; $n=3$ donors, $^{*}P<0.05$. (**C**) Alizarin Red staining of osteogenic hMSCs and (**F**) Oil Red O staining of adipogenic hMSCs after 10 days of differentiation. Scale bars: 50 μm.

on surfaces of varying ligand lateral spacing is of interest in the basic understanding of cellular mechanisms but is also relevant to the colonization of scaffolds for tissue engineering, showing that the ligand spacing on scaffolds could be tuned in order to maximize migration of hMSCs through, and thus increase colonization of, biomaterial constructs.

We also observed that osteogenic differentiation was enhanced on 34-nm-spaced RGD, whereas there was more adipogenic differentiation on 62-nm-spaced RGD. In addition, when cultured in mixed osteo- and adipogenic medium, hMSCs on 34 nm spacings tended to become osteogenic whereas those on 62-nm-spaced surfaces tended to become adipogenic. This aligns well with the differences we observed in hMSC morphology on the different lateral spacings. Osteogenic cells are typically more spread than adipogenic cells and have thick actin bundles, whereas adipogenic cells are generally more rounded and have fewer stress fibres (McBeath et al., 2004; Rodriguez et al., 2004). Although hMSCs on the 62-nm-spaced RGD were not rounded, they had a decreased spread area and fewer stress fibres than those on the more closely spaced RGD. It is believed that strong actomyosin contractility is required for osteogenesis (Chen et al., 1997; McBeath et al., 2004), and so the prominent stress fibres and mature FAs in hMCS on the 34-nm-spaced peptide would provide the strong cytoskeleton and robust anchorage points necessary to generate these large forces. By contrast, it is unlikely that the immature focal contacts and unstructured actin filaments seen in hMSCs on 62-nm-spaced RGD would be able to support the levels of tension required.

In addition, the different adhesion structures observed with increasing RGD spacing are likely to have different compositions, which will affect downstream signalling cascades (Cavalcanti-Adam et al., 2007). FAK is one such component that is necessary for osteogenesis (Salasznyk et al., 2007a; Salasznyk et al., 2007b) and we have demonstrated that FAK levels are reduced in hMSCs on surfaces with increased RGD spacing. Components (such as RhoA and ROCK) or regulators of their activity (such as p190RhoGEF and p190RhoGEF) might also be differentially recruited to, or activated in, the different adhesion complexes (Zhai et al., 2003; Lavelin and Geiger, 2005). RhoA is required for FA maturation and stress fibre assembly (Ridley and Hall, 1992) and is known to promote osteogenic differentiation (McBeath et al., 2004) and so, although further work is required to confirm this, it is probable that RhoA activity is greater in hMSCs on 34-nm- than on 62-nm-spaced RGD. FAK also regulates RhoA via direct binding and phosphorylation of p190RhoGAP and p190RhoGEF (Watanabe et al., 1999; Zhai et al., 2003; Schober et al., 2007), and so the reduced levels of FAK in hMSCs as RGD spacing increases also support this suggestion.

In many ways, our results are analogous to the outcomes seen when hMSCs are cultured on substrates of varying elasticity. Cells cultured on stiff substrates had larger FAs, a more contractile cytoskeleton and were more osteogenic than those cultured on soft substrates (which were more adipogenic) (Engler et al., 2006). In that study, the differences were attributed to a requirement for the force generated internally by a cell to be balanced by the force with which it can pull against the

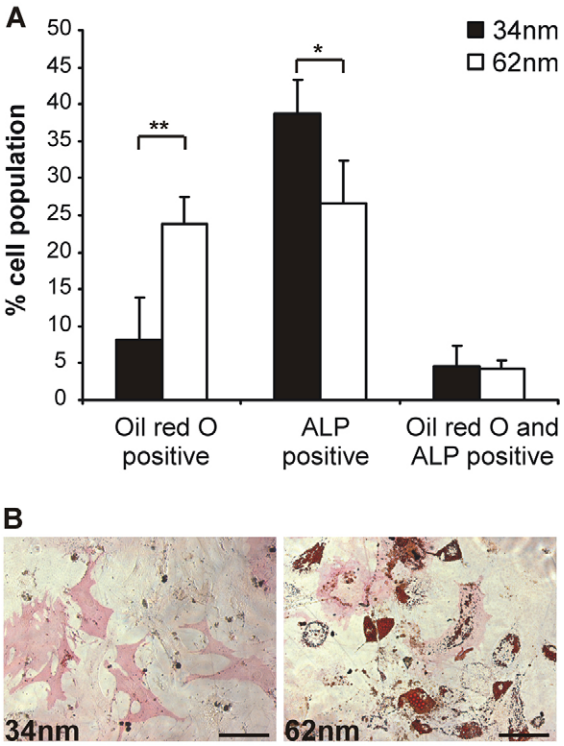

Fig. 7. Differentiation of hMSCs on different RGD peptide spacings. **(A)** Percentage of cells positive for alkaline phosphatase (ALP) and Oil Red O after seeding onto either 34-nm- or 62-nm-spaced peptides and culturing for 10 days. (**B**) Alkaline phosphatase (pink) and Oil Red O (red) staining of hMSCs cultured for 10 days in mixed osteo-adipogenic media. Scale bars: 50 μm.

underlying substrate (meaning that soft substrates could not support large contractile forces). In the case of lateral presentation of adhesion ligand, we hypothesize that the differences are a direct result of the reduced ability of integrins to cluster when RGD spacing is increased, leading to a reduced ability to form FAs and subsequent changes in cytoskeletal organization. Supporting this hypothesis, previous work has demonstrated that reducing the number of points at which the cell can contact the matrix decreases cytoskeletal tension and reduces osteogenic potential (Kilian et al., 2010).

Our findings show, for the first time, that the lateral spacing of adhesion peptides influences stem cell behaviour. We demonstrate that hMSCs can sense changes in the lateral spacing of an RGD adhesion peptide ranging from 34 to 62 nm and that this not only alters their ability to spread, form mature FAs and assemble stress fibres, but also affects motility and lineage specification. In the presence of induction media, osteogenic differentiation was increased on surfaces with smaller distances between the presented peptides, whereas adipogenic differentiation was enhanced when RGD spacing reached 62 nm. In addition, a mixed media containing cues sufficient to induce both osteo- and adipogenesis supported significantly more osteogenesis on 34 nm surfaces whereas significantly more adipocytes were present on 62-nm-spaced RGD. We hypothesize that the increased RGD spacing inhibited the clustering of integrins, a necessary step for mature FA formation and stress fibre assembly, which is essential for generating the actomyosin contractility associated with osteogenic differentiation. This opens up a new mechanism through which hMSCs are able to sense and respond to the physical environment and highlights an additional feature of the microenvironment that could be adapted to achieve specific outcomes for tissue engineering purposes.

Materials and Methods

Preparation of block copolymer surfaces

PS-PEO copolymer with 51 kDa PS block and 11.5 kDa PEO block (Polymer Source, Montreal, Canada) was maleimide-functionalized as described previously (George et al., 2009b). This was made up as a 1% (w/v) solution in toluene (Sigma-Aldrich) and blended in different ratios with a 1% (w/v) solution of PS (210 kDa from Polymer Source). Glass coverslips were prepared by exposure to UV and ozone for 10 minutes, followed by boiling in benzyl alcohol (Sigma) for 4 hours, rinsing in isopropanol and drying under a stream of nitrogen. Thin films were produced on the coverslips by spin-casting polymer blends onto the glass coverslips for 30 seconds at 600 ***g***. The surfaces were sterilised in 70% ethanol before binding of CGRGDS or CCRGES peptides (GenScript) to the maleimide via the terminal cysteine group. This was achieved by incubation of 100 μg/ml peptide in coupling buffer (0.1 M sodium phosphate, 0.15 M sodium chloride, 10 mM EDTA, pH 7.2) for 2 hours at room temperature. The surfaces were then washed thoroughly in PBS and blocked for a further 2 hours with 2% synperonic F108 (Fluka) prior to cell attachment. These are hereafter referred to as PS-PEO-Ma–RGD surfaces.

Cell culture

Human bone-marrow MSCs (hMSCs, kindly supplied by Gary Brooke at the Mater Medical Research Institute, Brisbane, Australia) were cultured in low-glucose DMEM supplemented with 100 U/ml penicillin, 100 μg/ml streptomycin (DMEM/ps) and 10% batch-tested foetal bovine serum (FBS) at 37℃ in 5% CO_2 in an atmosphere with 95% humidity. Upon reaching 70% confluence, hMSCs were passaged, replating at 2000 cells/cm^2. hMSCs were characterized by flow cytometry for expression of CD29, CD44, CD49a, CD73, CD90, CD105, CD146 and CD166 and were negative for CD34 and CD45. The cells displayed tri-lineage differentiation potential along the osteogenic, adipogenic and chondrogenic lineages as shown previously (Hudson et al., 2011). Integrin expression profiling showed expression of a broad range of integrin subunits, including high levels of integrins α1–α5 and αV as well as β1 integrin (supplementary material Fig. S1).

hMSCs were detached with TrypLE Select (Invitrogen), resuspended in 1% bovine serum albumin (BSA) in PBS then washed thoroughly prior to seeding onto PS-PEO-Ma–RGD surfaces in serum-free media (DMEM/ps and 1% ITS+; Sigma). For differentiation experiments, hMSCs were allowed to attach in serum-free conditions for 4 hours before exchanging the media for DMEM/ps containing 10% FBS plus osteogenic supplements (100 ng/ml dexamethasone, 50 μM ascorbate-2-phosphate and 10 mM β-glycerophosphate) or adipogenic supplements (1 μg/ml dexamethasone, 0.2 mM indomethacin, 0.5 mM isobutyl-1-methylxanthine and 10 μg/ml insulin). All experiments were performed using hMSCs from multiple donors between passages three and six.

Cell adhesion and integrin blocking assays

MSCs were seeded onto PS-PEO-Ma–RGD surfaces at a density of 5000 cells/cm^2 in serum-free media and allowed to attach for 2 hours. For integrin-blocking studies, MSCs were previously incubated in 0.1% BSA with integrin-blocking antibodies (α-integrin investigator kit ECM430 and β-integrin investigator kit ECM440 from Millipore, except for the β1-integrin antibody, clone MAR4 from Calbiochem) for 1 hour at 4℃. Attachment levels were determined by Crystal Violet assay. Briefly, cells were washed twice in PBS to remove unattached cells, fixed in 4% paraformaldehyde (Sigma-Aldrich, Sydney, Australia) for 20 minutes and stained with 0.1% (w/v) Crystal Violet (Sigma-Aldrich) in 200 mM 2-(*N*-morpholine) ethanesulfonic acid (Sigma-Aldrich), pH 6.0 for 10 minutes. Cells were washed five times in doubly distilled H_2O to remove excess Crystal Violet before addition of 100 μl of 10% glacial acetic acid. Absorbance was read at 590 nm using a Spectramax M5 Fluorometer (Molecular Devices).

Analysis of cell morphology, cytoskeleton and FA length

MSCs were cultured on PS-PEO-Ma–RGD surfaces at a density of 3,000 cells/cm^2 in serum-free media for periods of 4 and 24 hours, washed in PBS and fixed for 10 minutes in 4% paraformaldehyde. The cells were then permeabilized in 0.1% Triton X-100 in PBS for 5 minutes, blocked in 3% BSA and incubated with primary antibody at 4℃ overnight (1:600 anti-vinculin clone human Vin1, Sigma-Aldrich; 1:250 anti-FAK, Calbiochem). Incubation with secondary antibody (anti-mouse IgG–Alexa-Fluor-568), phalloidin–Alexa-Fluor-488 and Hoescht 33342 was performed for 1 hour at room temperature. Samples were rinsed thoroughly in PBS and mounted onto glass slides in Vectashield containing DAPI (Vector Laboratories). High resolution images were obtained using an LSR710 confocal microscope (Zeiss), with images for measurements of projected cell area,

circularity and FA length obtained using an Olympus IX81 microscope. The same exposure was used for images across all conditions, and images analysed using ImageJ 1.42 software (NIH, Bethesda, MD).

Cell migration

Cell migration was analysed using a multichannel migration device as previously described (Doran et al., 2009), see supplementary material Fig. S4. In brief, the device consists of a main inoculation chamber with migration channels protruding perpendicularly from it. In operation, the channel dimension and fluid surface tension prevent fluid from exiting the main chamber into the migration microchannels. It is thus possible to establish a confluent cell monolayer in the main chamber without any cell migration or media flow into the adjacent microchannel. Migration is then initiated by backfilling the microchannels with media, thus establishing a connection between the main chamber and the microchannel.

hMSCs were seeded onto the PS-PEO-Ma–RGD or TCP control surfaces within the devices' main chamber, at a density of 25,000 cells/cm^2 in serum-free media, and allowed to attach for a period of 4 hours. Migration channels (also presenting the PS-PEO-Ma–RGD or TCP control surfaces) were then backfilled with media to initiate migration and time zero pictures taken. Migration photographs and measurements were taken after a period of 24 hours.

Quantative real-time PCR

Total RNA was extracted using the RNeasy Minikit with on-column DNase treatment (Qiagen) according to the manufacturer's instructions, pooling cell lysates from three replicates per condition. cDNA was synthesized from 100 ng RNA using 200 U SuperScript III, or the equivalent volume of DNase- and RNase-free water for no-RT controls, in a total volume of 25 µl. Quantitative PCR (qPCR) reactions were set-up in a total volume of 10 µl with 1× Platinum SYBR Green qPCR SuperMix-UDG (Invitrogen) and 0.2 µM forward and reverse primers. A 7500 Fast Real-Time PCR System (Applied Biosystems) was used to run the samples, with fast cycling parameters of 2 minutes at 50℃ and 2 minutes at 95℃, then 40 cycles of 3 seconds at 95℃ and 30 seconds at 60℃, followed by a melt curve. Data was analysed using the $2^{-\Delta\Delta ct}$ method. GAPDH levels were unchanged across different lateral spacings and differentiation conditions (supplementary material Fig. S5) and therefore data was analysed using GAPDH as a housekeeping gene and normalizing back to day 0 expression levels.

Alkaline phosphatase *p*-nitrophenylphosphate assay

MSCs were seeded onto PS-PEO-Ma–RGD surfaces or control TCP surfaces at a density of 3000 cells/cm^2 in serum-free media for 4 hours then switched to osteogenic media. After 7 days, samples were collected by washing the cells in PBS and adding 150 µl of 0.1% TritonX-100 in 0.2 M carbonate buffer. Samples were fully lysed with three freeze–thaw cycles between −80℃ and 37℃. To determine alkaline phosphatase activity, 50 µl working substrate (0.3 mg/ml *p*-nitrophenylphosphate (Sigma) and 3.3 mM $MgCl_2$ in 0.2 M carbonate buffer) was added to each sample and incubated at 37℃ before measurement of the absorbance on a Spectramax M5 Fluorometer (Molecular Devices) with an excitation wavelength of 405 nm. The *p*-nitophenol concentration was determined by extrapolation form a standard curve and normalized to both incubation time and DNA content as assessed by PicoGreen assay (Molecular Probes, performed according to the manufacturer's instructions).

Histological staining

Alkaline phosphatase activity was detected by incubation for 5 minutes in 1 mg/ml Fast Red-TR (Sigma) and 0.2 mg/ml Napthol AS-MX phosphate (Sigma) in 0.1 M Tris-HCl, pH 9.2. von Kossa-positive mineralization was detected with a 30 minute incubation in 1% silver nitrate, followed by 5 minutes in 2.5% sodium thiosulphate (Sigma). Oil Red O staining was performed on cultures fixed in 4% paraformaldehyde using a 6:4 ratio of 0.5% Oil Red O (Sigma) in isopropanol to distilled H_2O.

Acknowledgements

This work was performed in part at the Queensland node of the Australian National Fabrication Facility, a company established under the National Collaborative Research Infrastructure Strategy to provide nano- and microfabrication facilities for Australia's researchers.

Funding

The authors would like to acknowledge funding from the Australian Research Council Discovery Grants Scheme [grant numbers DP1095429 and DP110104446].

Supplementary material available online at
http://jcs.biologists.org/lookup/suppl/doi:10.1242/jcs.087916/-/DC1

References

Arnold, M., Cavalcanti-Adam, E. A., Glass, R., Blummel, J., Eck, W., Kantlehner, M., Kessler, H. and Spatz, J. P. (2004). Activation of integrin function by nanopatterned adhesive interfaces. *Chem. Phys. Chem.* **5**, 383-388.

Arnold, M., Hirschfeld-Warneken, V. C., Lohmuller, T., Heil, P., Blummel, J., Cavalcanti-Adam, E. A., Lopez-Garcia, M., Walther, P., Kessler, H., Geiger, B. et al. (2008). Induction of cell polarization and migration by a gradient of nanoscale variations in adhesive ligand spacing. *Nano. Lett.* **8**, 2063-2069.

Arnold, M., Schwieder, M., Blummel, J., Cavalcanti-Adam, A., Lopez-Garcia, M., Kessler, H., Geiger, B. and Spatz, J. P. (2009). Cell interactions with hierarchically structured nano-patterned adhesive surfaces. *Soft Matter* **5**, 72-77.

Balaban, N. Q., Schwarz, U. S., Riveline, D., Goichberg, P., Tzur, G., Sabanay, I., Mahalu, D., Safran, S., Bershadsky, A., Addadi, L., et al. (2001). Force and focal adhesion assembly: a close relationship studied using elastic micropatterned substrates. *Nat. Cell Biol.* **3**, 466-472.

Cameron, A. R., Frith, J. E. and Cooper-White, J. J. (2011). The influence of substrate creep on mesenchymal stem cell behaviour and phenotype. *Biomaterials* **32**, 5979-5993.

Cavalcanti-Adam, E. A., Micoulet, A., Blummel, J., Auernheimer, J., Kessler, H. and Spatz, J. P. (2006). Lateral spacing of integrin ligands influences cell spreading and focal adhesion assembly. *Eur. J. Cell Biol.* **85**, 219-224.

Cavalcanti-Adam, E. A., Volberg, T., Micoulet, A., Kessler, H., Geiger, B. and Spatz, J. P. (2007). Cell spreading and focal adhesion dynamics are regulated by spacing of integrin ligands. *Biophys. J.* **92**, 2964-2974.

Chen, C. S., Mrksich, M., Huang, S., Whitesides, G. M. and Ingber, D. E. (1997). Geometric control of cell life and death. *Science* **276**, 1425-1428.

Choi, C. K., Vicente-Manzanares, M., Zareno, J., Whitmore, L. A., Mogilner, A. and Horwitz, A. R. (2008). Actin and alpha-actinin orchestrate the assembly and maturation of nascent adhesions in a myosin II motor-independent manner. *Nat. Cell Biol.* **10**, 1039-1050.

Chollet, C., Chanseau, C., Remy, M., Guignandon, A., Bareille, R., Labrugere, C., Bordenave, L. and Durrieu, M. C. (2009). The effect of RGD density on osteoblast and endothelial cell behavior on RGD-grafted polyethylene terephthalate surfaces. *Biomaterials* **30**, 711-720.

Critchley, D. R. (2000). Focal adhesions - the cytoskeletal connection. *Curr. Opin. Cell Biol.* **12**, 133-139.

Cukierman, E., Pankov, R., Stevens, D. R. and Yamada, K. M. (2001). Taking cell-matrix adhesions to the third dimension. *Science* **294**, 1708-1712.

Doran, M. R., Mills, R. J., Parker, A. J., Landman, K. A. and Cooper-White, J. J. (2009). A cell migration device that maintains a defined surface with no cellular damage during wound edge generation. *Lab Chip* **9**, 2364-2369.

Engler, A. J., Sen, S., Sweeney, H. L. and Discher, D. E. (2006). Matrix elasticity directs stem cell lineage specification. *Cell* **126**, 677-689.

Geiger, B. and Bershadsky, A. (2001). Assembly and mechanosensory function of focal contacts. *Curr. Opin. Cell Biol.* **13**, 584-592.

George, P. A. and Cooper-White, J. J. (2009). Kinetically constrained block copolymer self-assembly a simple method to control domain size. *Eur. Polym. J.* **45**, 1065-1071.

George, P. A., Donose, B. C. and Cooper-White, J. J. (2009a). Self-assembling polystyrene-block-poly(ethylene oxide) copolymer surface coatings: resistance to protein and cell adhesion. *Biomaterials* **30**, 2449-2456.

George, P. A., Doran, M. R., Croll, T. I., Munro, T. P. and Cooper-White, J. J. (2009b). Nanoscale presentation of cell adhesive molecules via block copolymer self-assembly. *Biomaterials* **30**, 4732-4737.

Huang, J., Grater, S. V., Corbellini, F., Rinck, S., Bock, E., Kemkemer, R., Kessler, H., Ding, J. and Spatz, J. P. (2009). Impact of order and disorder in RGD nanopatterns on cell adhesion. *Nano. Lett.* **9**, 1111-1116.

Hudson, J. E., Mills, R. J., Frith, J. E., Brooke, G., Jaramillo-Ferrada, P., Wolvetang, E. J. and Cooper-White, J. J. (2011). A defined medium and substrate for expansion of human mesenchymal stromal cell progenitors that enriches for osteo- and chondrogenic precursors. *Stem Cells Dev.* **20**, 77-87.

Humphries, M. J., McEwan, P. A., Barton, S. J., Buckley, P. A., Bella, J. and Mould, A. P. (2003). Integrin structure: heady advances in ligand binding, but activation still makes the knees wobble. *Trends Biochem. Sci.* **28**, 313-320.

Hynes, R. O. (1992). Integrins: versatility, modulation, and signaling in cell adhesion. *Cell* **69**, 11-25.

Irvine, D. J., Hue, K. A., Mayes, A. M. and Griffith, L. G. (2002). Simulations of cell-surface integrin binding to nanoscale-clustered adhesion ligands. *Biophys. J.* **82**, 120-132.

Kantawong, F., Burgess, K. E., Jayawardena, K., Hart, A., Burchmore, R. J., Gadegaard, N., Oreffo, R. O. and Dalby, M. J. (2009). Whole proteome analysis of osteoprogenitor differentiation induced by disordered nanotopography and mediated by ERK signalling. *Biomaterials* **30**, 4723-4731.

Kilian, K. A., Bugarija, B., Lahn, B. T. and Mrksich, M. (2010). Geometric cues for directing the differentiation of mesenchymal stem cells. *Proc. Natl. Acad. Sci. USA* **107**, 4872-4877.

Klees, R. F., Salasznyk, R. M., Kingsley, K., Williams, W. A., Boskey, A. and Plopper, G. E. (2005). Laminin-5 induces osteogenic gene expression in human mesenchymal stem cells through an ERK-dependent pathway. *Mol. Biol. Cell* **16**, 881-890.

Kuhlman, W., Taniguchi, I., Griffith, L. G. and Mayes, A. M. (2007). Interplay between PEO tether length and ligand spacing governs cell spreading on RGD-modified PMMA-g-PEO comb copolymers. *Biomacromolecules* **8**, 3206-3213.

Kundu, A. K. and Putnam, A. J. (2006). Vitronectin and collagen I differentially regulate osteogenesis in mesenchymal stem cells. *Biochem. Biophys. Res. Commun.* **347**, 347-357.

Lavelin, I. and Geiger, B. (2005). Characterization of a novel GTPase-activating protein associated with focal adhesions and the actin cytoskeleton. *J. Biol. Chem.* **280**, 7178-7185.

Maheshwari, G., Brown, G., Lauffenburger, D. A., Wells, A. and Griffith, L. G. (2000). Cell adhesion and motility depend on nanoscale RGD clustering. *J. Cell Sci.* **113**, 1677-1686.

Martino, M. M., Mochizuki, M., Rothenfluh, D. A., Rempel, S. A., Hubbell, J. A. and Barker, T. H. (2009). Controlling integrin specificity and stem cell differentiation in 2D and 3D environments through regulation of fibronectin domain stability. *Biomaterials* **30**, 1089-1097.

Massia, S. P. and Hubbell, J. A. (1991). An RGD spacing of 440 nm is sufficient for integrin alpha V beta 3-mediated fibroblast spreading and 140 nm for focal contact and stress fiber formation. *J. Cell Biol.* **114**, 1089-1100.

McBeath, R., Pirone, D. M., Nelson, C. M., Bhadriraju, K. and Chen, C. S. (2004). Cell shape, cytoskeletal tension, and RhoA regulate stem cell lineage commitment. *Dev. Cell* **6**, 483-495.

Nelson, C. M., Jean, R. P., Tan, J. L., Liu, W. F., Sniadecki, N. J., Spector, A. A. and Chen, C. S. (2005). Emergent patterns of growth controlled by multicellular form and mechanics. *Proc. Natl. Acad. Sci. USA* **102**, 11594-11599.

Palecek, S. P., Loftus, J. C., Ginsberg, M. H., Lauffenburger, D. A. and Horwitz, A. F. (1997). Integrin-ligand binding properties govern cell migration speed through cell-substratum adhesiveness. *Nature* **385**, 537-540.

Poole, K., Khairy, K., Friedrichs, J., Franz, C., Cisneros, D. A., Howard, J. and Mueller, D. (2005). Molecular-scale topographic cues induce the orientation and directional movement of fibroblasts on two-dimensional collagen surfaces. *J. Mol. Biol.* **349**, 380-386.

Ren, X. D., Kiosses, W. B. and Schwartz, M. A. (1999). Regulation of the small GTP-binding protein Rho by cell adhesion and the cytoskeleton. *EMBO J.* **18**, 578-585.

Ridley, A. J. and Hall, A. (1992). The small GTP-binding protein rho regulates the assembly of focal adhesions and actin stress fibers in response to growth factors. *Cell* **70**, 389-399.

Riveline, D., Zamir, E., Balaban, N. Q., Schwarz, U. S., Ishizaki, T., Narumiya, S., Kam, Z., Geiger, B. and Bershadsky, A. D. (2001). Focal contacts as mechanosensors: externally applied local mechanical force induces growth of focal contacts by an mDia1-dependent and ROCK-independent mechanism. *J. Cell Biol.* **153**, 1175-1186.

Rodriguez, J. P., Gonzalez, M., Rios, S. and Cambiazo, V. (2004). Cytoskeletal organization of human mesenchymal stem cells (MSC) changes during their osteogenic differentiation. *J. Cell. Biochem.* **93**, 721-731.

Rowlands, A. S., George, P. A. and Cooper-White, J. J. (2008). Directing osteogenic and myogenic differentiation of MSCs: interplay of stiffness and adhesive ligand presentation. *Am. J. Physiol. Cell Physiol.* **295**, C1037-C1044.

Ruiz, S. A. and Chen, C. S. (2008). Emergence of patterned stem cell differentiation within multicellular structures. *Stem Cells* **26**, 2921-2927.

Ruoslahti, E. (1996). RGD and other recognition sequences for integrins. *Annu. Rev. Cell Dev. Biol.* **12**, 697-715.

Salasznyk, R. M., Klees, R. F., Hughlock, M. K. and Plopper, G. E. (2004). ERK signaling pathways regulate the osteogenic differentiation of human mesenchymal stem cells on collagen I and vitronectin. *Cell Commun. Adhes.* **11**, 137-153.

Salasznyk, R. M., Klees, R. F., Boskey, A. and Plopper, G. E. (2007a). Activation of FAK is necessary for the osteogenic differentiation of human mesenchymal stem cells on laminin-5. *J. Cell. Biochem.* **100**, 499-514.

Salasznyk, R. M., Klees, R. F., Williams, W. A., Boskey, A. and Plopper, G. E. (2007b). Focal adhesion kinase signaling pathways regulate the osteogenic differentiation of human mesenchymal stem cells. *Exp. Cell Res.* **313**, 22-37.

Schober, M., Raghavan, S., Nikolova, M., Polak, L., Pasolli, H. A., Beggs, H. E., Reichardt, L. F. and Fuchs, E. (2007). Focal adhesion kinase modulates tension signaling to control actin and focal adhesion dynamics. *J. Cell Biol.* **176**, 667-680.

Selhuber-Unkel, C., Lopez-Garcia, M., Kessler, H. and Spatz, J. P. (2008). Cooperativity in adhesion cluster formation during initial cell adhesion. *Biophys. J.* **95**, 5424-5431.

Selhuber-Unkel, C., Erdmann, T., Lopez-Garcia, M., Kessler, H., Schwarz, U. S. and Spatz, J. P. (2010). Cell adhesion strength is controlled by intermolecular spacing of adhesion receptors. *Biophys. J.* **98**, 543-551.

von Wichert, G., Haimovich, B., Feng, G. S. and Sheetz, M. P. (2003). Force-dependent integrin-cytoskeleton linkage formation requires downregulation of focal complex dynamics by Shp2. *EMBO J.* **22**, 5023-5035.

Watanabe, N., Kato, T., Fujita, A., Ishizaki, T. and Narumiya, S. (1999). Cooperation between mDia1 and ROCK in Rho-induced actin reorganization. *Nat. Cell Biol.* **1**, 136-143.

Winer, J. P., Janmey, P. A., McCormick, M. E. and Funaki, M. (2009). Bone marrow-derived human mesenchymal stem cells become quiescent on soft substrates but remain responsive to chemical or mechanical stimuli. *Tissue Eng. Part A* **15**, 147-154.

Yim, E. K., Darling, E. M., Kulangara, K., Guilak, F. and Leong, K. W. (2010). Nanotopography-induced changes in focal adhesions, cytoskeletal organization, and mechanical properties of human mesenchymal stem cells. *Biomaterials* **31**, 1299-1306.

Zhai, J., Lin, H., Nie, Z., Wu, J., Canete-Soler, R., Schlaepfer, W. W. and Schlaepfer, D. D. (2003). Direct interaction of focal adhesion kinase with p190RhoGEF. *J. Biol. Chem.* **278**, 24865-24873.

Journal of Cell Science